Journal of Environmental Chemical Engineering 11 (2023) 110574

Contents lists available at ScienceDirect

Journal of Environmental Chemical Engineering

journal homepage: www.elsevier.com/locate/jece

Evaluation of new photochemical systems for water disinfection by the integration of particle tracking into kinetic models for microbial inactivation

Cintia Casado, Verónica Yunta, Javier Marugán *

Department of Chemical and Environmental Technology, ESCET, Universidad Rey Juan Carlos, C/ Tulipán s/n, Móstoles, 28933 Madrid, Spain

ARTICLE INFO

Editor: Despo Kassinos

Keywords:
CFD
UV
Dose
Virus
Photoreactor
Microbial trajectories

ABSTRACT

This work presents the development of a novel methodology for the simulation of photochemical processes for water disinfection using computational fluid dynamics (CFD). A new approach was implemented to calculate and visualise the disinfection performance as the microorganisms move along the photoreactor. Hydrodynamics and microorganism's statistical trajectories were computed using the discrete phase model, which also provides the distribution of microbial residence times. The distribution of radiation in the reactor was calculated using the discrete ordinate method. The local values of incident radiation were integrated over each statistical trajectory path to get the accumulated dose received for each microbial particle. The coupling in situ of the cumulative radiation dose with the inactivation kinetics allows monitoring of the disinfection process concurrently with the particle tracking. This methodology introduces significant advantages over the traditional estimation of the microorganism inactivation sequentially after calculating the dose histograms estimated from the statistical trajectories. The developed tool enables evaluating the photoreactor efficiency in each reactor position, a useful capability for optimising and scaling up complex geometries. It also allows the easy, intuitive visualisation of microbial inactivation trajectories, improving the understanding of the influence of the reactor features on the disinfection process. Application of this computational approach to two different photoreactor geometries using a virus as a representative target microbe is presented.

1. Introduction

Drinking water shortage is a worldwide problem [1]. Water safety is commonly compromised by microorganisms that can cause waterborne diseases to the consumer [2]. UV disinfection has attracted the attention of the water treatment industry. Exposure of microorganisms to UV-C germicidal radiation can lead to the inactivation of a wide range of pathogens without the formation of disinfection by-products [3].

The performance of a UV disinfection reactor is based on the actual UV radiation received by the microorganisms present in the treated water. For this reason, it is critical to guarantee that the residence time distribution and the radiation field inside the reactor volume ensure that all the microbial particles receive the required threshold level of radiation. Microbial inactivation kinetics depends on the incident radiation and exposure time, both combined into the accumulated radiation dose. For reactors with simple geometries, it can be considered that microbes are homogeneously distributed in the reactor volume. However, for complex geometries (with preferential routes, some degree of vorticity, or when dead zones are present), it becomes necessary to integrate radiation distribution and microbial trajectory to calculate the radiation dose received by the microbial population accurately.

Computer-assisted simulation enables scale-up and evaluates the impact of new technologies at a minimal cost. It avoids investments in the implementation of technologies that have not reached a sufficient degree of maturity and gives the possibility of optimising the design, being an ideal tool to enhance research results with potential industrial applications. Computational fluid dynamics (CFD) multiphysics modelling allows integrating diverse physical-chemical processes occurring in photoactivated reactors, such as fluids flow, radiation transport, mass transfer and reaction kinetics. Specifically, it can compute the statistical distribution of microbial trajectories using the discrete phase method. This method uses a Lagrangian approach to calculate the most probable microbial path over a calculated flow field [4].

* Corresponding author.
E-mail address: javier.marugan@urjc.es (J. Marugán).

https://doi.org/10.1016/j.jece.2023.110574
Received 9 May 2023; Received in revised form 30 June 2023; Accepted 15 July 2023
Available online 19 July 2023

A rigorous calculation of irradiance distribution is also critical when the reactor's geometry is complicated or when the lighting sources generate intricate radiation patterns inside the reactor, such as the non-homogeneous light distribution provided by LED [5]. Accurate light distribution and spatial incident radiation field inside the photoreactor volume can be computed by solving the radiative transfer equation using the discrete ordinates method available in standard CFD packages.

Significant efforts have been devoted to the analysis of radiation distribution with microbial trajectories using CFD tools [6–9]. In some cases, the calculated UV dose distribution has been used in the form of frequency histograms to calculate the global disinfection performance of the reactor by feeding the data to kinetic models for the inactivation of specific microbial targets [10,11]. In those cases, inactivation results have been calculated sequentially, considering the photoreactor as a black box with the specific distribution of UV doses preliminary calculated by CFD modelling.

This work presents a novel methodology for the coupling of radiation dose calculation with the microbial inactivation kinetics along the microbial trajectories. The integration of the reaction kinetics in situ with the radiation transport and the particle tracking allows the visual monitorisation of the disinfection rates in different reactor regions. This methodology makes possible the calculation of the inactivation efficiency along the different microbial trajectories. Consequently, a more in-depth analysis of the disinfection process inside the reactor is provided, not only the global average behaviour. The developed model has been applied to analyse the inactivation of MS2 virus in water using two UV photoreactors with different geometry and light sources. This method constitutes a powerful tool for optimising the photoreactor design. The geometry and UV sources could be finely tuned to reduce the impact of regions with low disinfection rates resulting from the combination of flow and radiation fields.

2. Computational model

All the simulations were carried out using ANSYS software v.14.5.

2.1. Geometry and mesh of the photoreactors

2.1.1. Tubular photoreactor

The tubular reactor is illuminated externally with LEDs and using and includes a reflective to improve the homogeneity of the available light. This reactor allows studying the effect of the LEDs distribution and light intensity with a simple geometry regarding the velocity field (a tubular pipe). The tubular reactor modelled has an internal diameter of 50 mm, 500 mm length and an internal volume of 0.98 L illuminated with LED sources. Four different LED design configurations (Table 1), distributed along an 80 mm diameter aluminium pipe, were used to study their effect on the microbial inactivation distribution. The aluminium wall reflects light back to the reactor volume, increasing the optical path and incident radiation availability. The air region between the light source and the reactor window is required for the LED's cooling. The discretisation meshes varied slightly among the designs, having all of them around 1 million cells, with significant refinement near the LEDs to correctly capture the emission shape. This number of cells is high enough to provide mesh-independent results for the radiation model, the field requiring greater computational resources. However, this initial mesh is too thick in the internal part (the reactor itself, where the water flows, see Fig. 1**A**) to correctly capture the velocity profile close to the reactor walls. For this reason, a second mesh was done only for the water pipe for the calculation of fluid dynamics and particle tracking and radiation, where radiation results are interpolated from the previous mesh. Due to the symmetry plane, only half of the reactor needs to be modelled. Carrying out the symmetry reduces the number of cells by half and thereby reduces the computational cost.

Table 1
LED configurations studied for the tubular reactor.

Name	Number of LEDs	Distribution	
		Columns	Rows
Design A1	12	3	4
Design A2	24	3	8
Design A3	48	6	8
Design A4	72	9	8

2.1.2. Annular photoreactor

The annular configuration illuminated internally with a tubular lamp is one of the most common photoreactor designs used in photoactivated processes to maximise energy efficiency in the use of the light emitted by tubular lamps. On the other hand, in this geometry (Fig. 1**B**), the configuration of inlet and outlet tube pipes generates a complex velocity field, with inhomogeneous flow and the presence of dead zones, the reason why this reactor is selected to study the influence of the velocity field in the inactivation results. The annular photoreactor modelled has an internal diameter of 30 mm, an external diameter of 50 mm, and a total length of 150 mm. The inlets (tilted 45° angle to favour mixing) have 6 mm diameter inlet and outlet pipe. The illuminated volume is 0.1885 L. A tubular UV-C mercury lamp is placed on the axis of the reactor. A spatial discretisation mesh of approximately 840,000 elements was used (Fig. 1**B**). More details about this photoreactor can be founded elsewhere [12]. As this reactor's geometry strongly influences the presence of an inhomogeneous velocity field, four different flow rates were studied (Table 2).

2.2. Flow field

Hydrodynamics calculations have been carried out considering a three-dimensional and steady-state flow through the resolution of the continuity equation and the classical Navier-Stokes equation. The fluid was assumed to be Newtonian, incompressible, and isothermal, with constant physical properties at 25ºC.

The **tubular photoreactor's** inlet average velocity was set to 0.0283 $m \cdot s^{-1}$ (3.33 $L \cdot min^{-1}$), normal to the boundary surface and simulated with laminar flow. As the flow is expected to come from a large pipe, developed velocity profile is set at the inlet boundary.

For the **annular photoreactor**, the average velocity at the inlet surface was modified according to Table 2, also normal to the boundary surface. The standard turbulent k-ε model with scalable wall functions was used (details elsewhere [13]). At the outlet, atmospheric pressure was applied in both reactors. A no-slip boundary condition was imposed at all reactor walls.

2.3. Particle tracking

The discrete phase model (DPM) was used to calculate the microbial residence time distribution, commonly called particle tracking. This model uses a Lagrangian approach, in which a dispersed phase is solved by tracking a large number of particles through the calculated flow field. In general, the dispersed phase could exchange momentum, mass, and energy with the fluid phase. However, in this case, microbial particles can be assumed to be inert, small enough to move entirely with the fluid. An uncoupled DPM was used with postprocessing purposes, being the flow not affected by the presence of the particles. The density of microorganisms was considered the same as the carrier fluid (water). A detailed description of the discrete phase model's equations can be founded elsewhere [13]. Particles with a diameter of $5 \cdot 10^{-6}$ m were injected into the inlet boundary. Previous studies have demonstrated that in the Lagrangian framework, results are not affected by the particle diameter [6,11,14,15].

The number of particles injected into the inlet was 1221 for the tubular reactor and 126 for the annular reactor, equal to the number of cells at the inlet surface (which corresponds to a density of 4.45 and 0.6

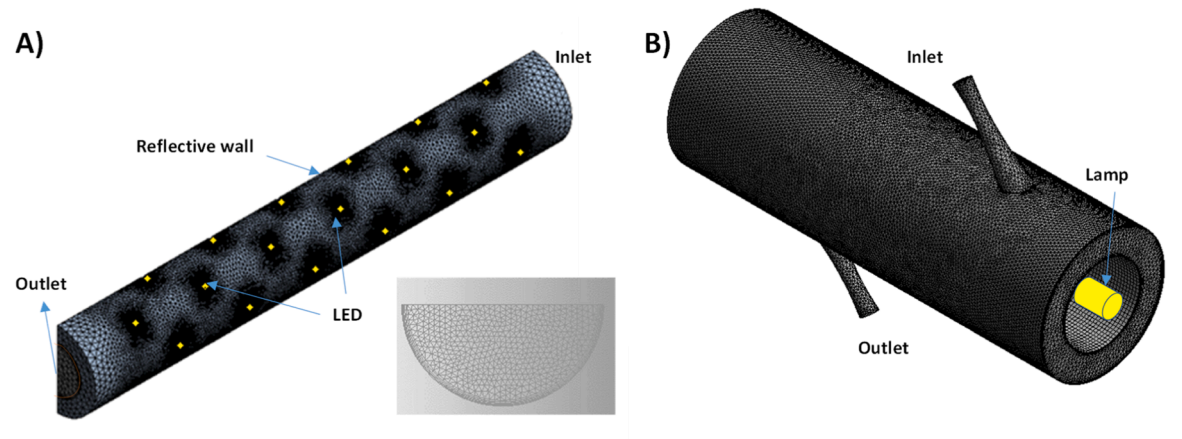

Fig. 1. Geometry and spatial discretisation mesh of the photoreactors. A) Tubular photoreactor with 48 LED (design A3) and detail of the pipe walls refinement. B) Annular photoreactor.

Table 2
Flow rates studied for the annular reactor.

Name	Flow rate (L·min^{-1})	Inlet velocity (m·s)
Design B_V1	2.62	1.543
Design B_V2	1.31	0.770
Design B_V3	0.87	0.514
Design B_V4	0.66	0.386

million of trajectories per m^2). These values have been optimised to get results independent on the number of particles, which are injected on the mesh cells of the inlet surface and follow the calculated flow lines. A higher number doesn't provide higher accuracy, whereas increases unnecessary the computational time.

2.4. UV radiation field

The radiation field was calculated using the Discrete Ordinate Method (DOM). The incident radiation in each spatial cell is calculated by integrating the radiation intensity in the spherical space directions. The method starts by creating a discretisation of spatial directions (quadrature) and solves the Radiative Transfer Equation (RTE) in each one. Details about the RTE and DOM can be founded elsewhere [12]. For the low temperatures at which the photoactivated processes take place, thermal emission can be neglected. Therefore, the temperature was fixed to 1 K to inactivate this calculation in the radiation simulations (fluid dynamics is calculated with fluid properties at 25 ºC). Based on previous studies [16], an angular discretisation of 15 × 15 divisions in theta and phi angle for each sphere octant was used for radiation calculations.

For the **tubular photoreactor**, the LEDs were simulated as planar surfaces with a maximum emission peak at 280 nm, and a radiant flow of 11 mW, corresponding to an emission flux of 1992 W m^{-2}. LEDs have an expanded opening (viewing angle) of about 120°. The aluminium surface has a reflectance of 0.85 with 10% of diffuse fraction.

The **annular photoreactor** is illuminated with a UV-C mercury lamp of 16 mm in diameter, 210 mm length. The lamp surface has an isotropic emission flux of 93.1 W m^{-2}. All surfaces have been declared transparent to light (full direct transmission).

2.5. Inactivation kinetics

MS2 virus has been selected as the model target microorganism for the evaluation of the developed methodology. MS2 is one of the recommended microorganisms for evaluating UV reactors' disinfection [17], as it has a relatively high UV resistance [8]. Its dose-response for UV inactivation can be described by conventional first-order Chick-Watson kinetics adapted for UV disinfection [10,11]:

$$\frac{N}{N_0} = f(D) = 10^{(-k_1 D + k_2)} \quad (1)$$

where N/N_0 is the normalised concentration of surviving microorganisms, D is the fluence or UV dose (J m^{-2}), and k_1 and k_2 are the kinetic constants whose values can be obtained from the literature [11,18] (k_1 = 0.0064 m^2 J^{-1} and k_2 = 0.361).

Despite its limitation to accurately predict dynamic survival patterns of more complex cellular microorganism such as bacteria [19,20], first-order Chick-Watson equation is commonly used to fit experimental data and estimate the microbial inactivation rate of viruses, being therefore very useful to showcase the capabilities of the presented methodology without the need for further mechanistic kinetic approaches.

The dose (J m^{-2}) received by each particle is calculated as the integral over time of the incident radiation (W m^{-2}) along the particle path. The incident radiation is also called fluence rate, which is the radiation reaching a microbial particle from all the spherical space of directions. The dose calculation was carried out using a user-defined subroutine.

Previous studies used the histogram of UV dose to calculate the concentration of surviving microorganisms according to Eq. (2):

$$\frac{N}{N_0} = \int_0^{\infty} f(D)\cdot E(D)\cdot dD \quad (2)$$

where *E(D)* is the frequency of particles with a specific dose value and *f (D)* is the MS2 dose-response for UV inactivation described in Eq. (1).

In contrast, the methodology presented in this work introduces Eq. (1) directly into the CFD model, being calculated in-situ the microbial inactivation as the evolution of N/N_0 along each trajectory using a user-defined function (Appendix A).

2.6. Convergence criteria and solution strategy

The governing equations were solver using the segregated steady-state solver. Second-order upwind discretisation scheme was employed except for pressure for which the standard method was selected. The SIMPLE algorithm was chosen for the pressure–velocity coupling. The convergence of the numerical solution was ensured by monitoring the scaled residuals to a criterion of at least 10^{-6} for the continuity, momentum variables and incident radiation. Additionally, the variables of interest have been monitored at different surfaces of the computational domain as an indicator of convergence (at least 50 iterations without changes)., The model was solved in steady state in three

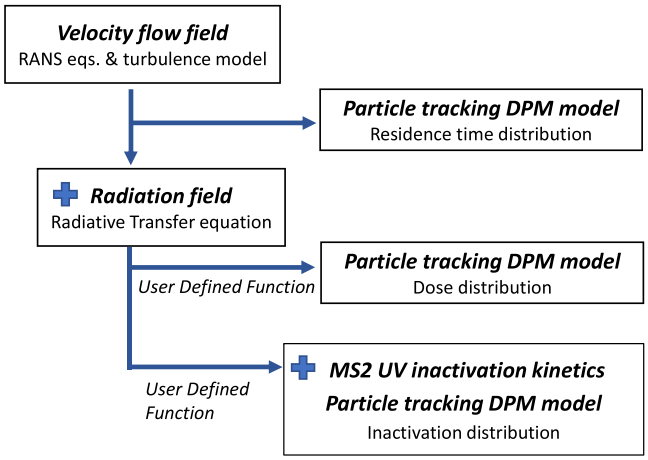

Fig. 2. Model solution strategy.

steps. Fig. 2 show the solution strategy. First, the flow field is solved in the Eulerian framework (equations of conservation of mass and momentum in each cell). After this step, the residence time distribution is obtained tracking particle trajectories. Second, the radiation field is solved, and then, using both fields, the radiation dose distribution is calculated for the particles pathlines. Finally, the discrete phase model is applied again (including disinfection kinetics) to calculate in situ inactivation. Table 3 summarises all the boundary conditions used in the model.

2.7. Data analysis

The results have been analysed in the form of pathlines of the selected property within the photoreactor as well as in the form of histograms (density function, DF, frequency of each value obtained, in % against the value) in the outlet section of the reactor, although the developed tool would allow obtaining results on any plane. Results are flow-averaged to obtain statistical data from the histograms. In tubular pipes, particles with the longest residence time (and, therefore, also dose and inactivation) correspond to trajectories close to the walls that will have lower velocity (tending to cero). Additionally, close to the walls usually the cell density increases. For this reason, the mean values are obtained weighted according to the flow rate, reducing the importance of the trajectories close to the wall according to Eq. (3):

$$< DF >= \frac{\sum_{faces} (\overrightarrow{Area_i} \cdot \overrightarrow{v_i}) DF_i}{\sum_{faces} (\overrightarrow{Area_i} \cdot \overrightarrow{v_i})} \quad (3)$$

From the cumulative density function, quartiles are obtained as follows:

- The first quartile: $P(X \leq Q1) = 0.25$. The value at which 25% of the probability distribution is below it.
- The second quartile: $P(X \leq Q2) = 0.50$. The value at which 50% of the probability distribution is below it.
- The third quartile: $P(X \leq Q3) = 0.75$. The value at which 75% of the probability distribution is below it.

Additionally, the min value of the ND, quartile 90% and 99%, and the relative standard deviation (RSD) have been calculated to compare different cases.

3. Results

3.1. Tubular reactor

The flow field for the tubular reactor was solved for an average inlet velocity of 0.0283 $m \cdot s^{-1}$ set as an inlet boundary. The histogram of residence time distribution for the tubular photoreactor obtained with the discrete phase model is shown in Fig. 3, showing good agreement with the calculated E(t) curve for an ideal laminar flow having the same average velocity [21] (red line in Fig. 3). The tubular reactor has an average residence time of 18.31 s (the space-time calculated with the mean velocity is 17.67 s), being the minimum of 9.10 s (in the pipe centre). The maximum value is not relevant since the residence time will tend to infinity near the walls where velocity tends to zero. It is a positive asymmetric distribution, 75% of the values are below 18.07 s (quartile 3) and 99% of the values are below 82.73 s (percentile 99).

Increasing the number of LEDs obviously increases the radiation reaching the reactor (see Fig. 4 A1-A4, with the results of incident radiation in the reactor volume for the different configurations of LEDs used for the tubular reactor). Table 4 includes the results of the average radiation reaching the reactor wall and its standard deviation, the

Table 3
Summary of boundary conditions.

	Momentum	Radiation	DPM
Tubular reactor 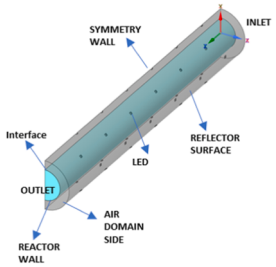	Inlet. Type: *velocity inlet*, normal to surface. Expression including developed profile. Outlet. Type: *pressure outlet*, atmospheric pressure. Reactor wall. Type: *wall*, No-slip conditions. Symmetry wall. Type: *symmetry* Air domain: velocity fixed to 0.	LED surface. Type: *Semi-transparent wall.* Diffuse irradiation. Beam width definition for LED viewing angle. Reflector Type: *Opaque wall.* Diffuse fraction 0. Internal emissivity 0.15. Inlet, Outlet, Air domain side, Reactor Wall. Type: *Semi-transparent wall* (all properties to 0, transparent to light) Symmetry wall. Type: symmetry Air and water domain: temperature fixed to 1 K.	Inlet. Type: *Escape* Outlet. Type: *Escape* Reactor wall. Type: *Reflect*
Annular reactor 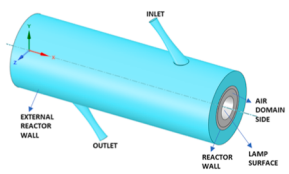	Inlet. Type: *velocity inlet*, normal to surface. k, ε definition Expression including developed profile. Outlet. Type: *pressure outlet*, atmospheric pressure. External Reactor wall, Reactor wall. Type: *wall*, No-slip conditions. Air domain: velocity fixed to 0.	Lamp surface. Type: *Semi-transparent wall.* Isotropic diffuse irradiation. Inlet, Outlet, Air domain side, Reactor Wall. Type: *Semi-transparent wall* (all properties to 0, transparent to light) Air and water domain: temperature fixed to 1 K.	Inlet. Type: *Escape* Outlet. Type: *Escape* Reactor wall, External reactor wall. Type: *Reflect*

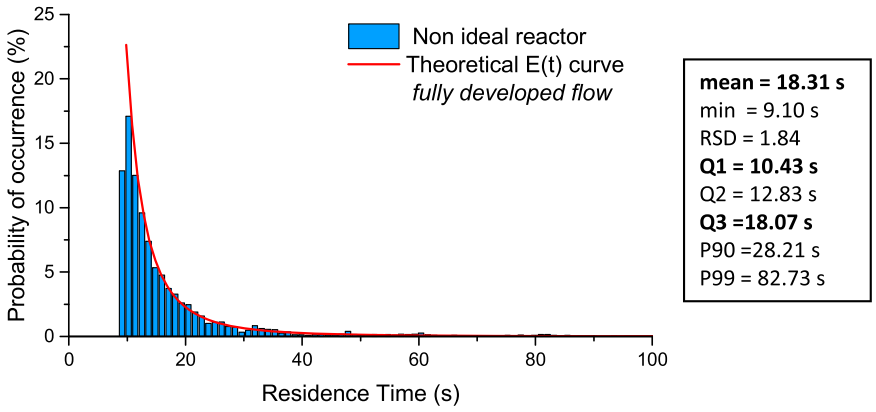

Fig. 3. Residence time distribution in the tubular reactor (design A) and E(t) curve for an ideal laminar flow.

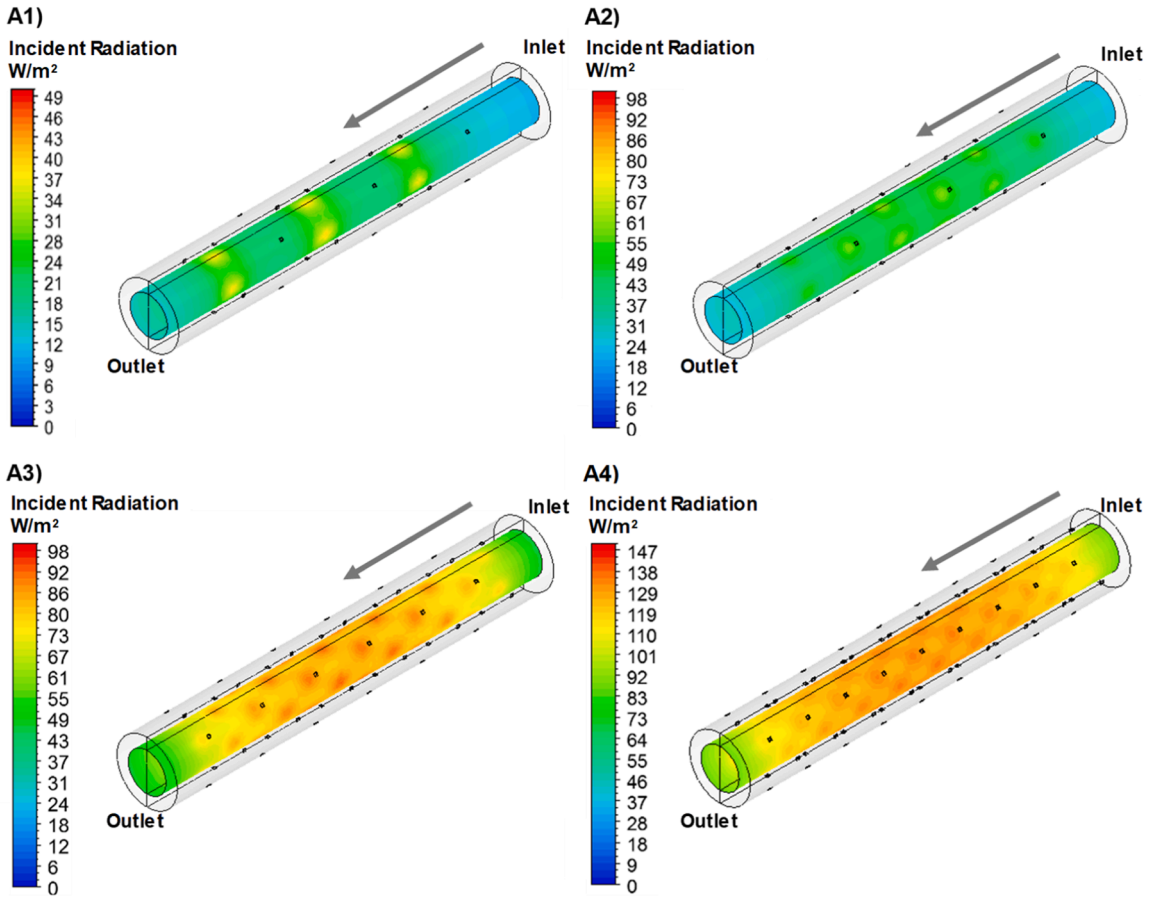

Fig. 4. Incident radiation in the tubular reactor illuminated with the four different LED configurations with A1) 12, A2) 24, A3) 48 and A4) 72 LEDs.

Table 4
Average incident radiation in the tubular reactor photoreactor.

Name	Incident Radiation at the wall ± SD ($W{\cdot}m^{-2}$)	Uniformity Index	Volume Average Incident Radiation ($W{\cdot}m^{-2}$)
Design A1	20.82 ± 27.4%	0.90	20.16
Design A2	41.71 ± 15.8%	0.92	40.40
Design A3	75.31 ± 11.15%	0.94	72.05
Design A4	120.61 ± 11.05%	0.96	115.95

uniformity index, and the average incident radiation in all the reactor volume, for the four studied configurations. The uniformity index, with a maximum value of 1, represents the degree of variation of the incident radiation on the reactor wall surface.

Even though LEDs are mounted over a reflective wall, the homogeneity calculated over the photoreactor wall only reaches a value comparable to the traditional tubular lamp (used in the annular photoreactor, as will be shown later), when the number of LEDs is

increased to at least 48 (Fig. 4 A3). The standard deviation decreases as the number of LEDs increases since the incident radiation is more homogeneous, being similar for 48 (A3) and 72 (A4) LEDs. It is important to remark that the homogeneity in the radiation distribution strongly affects the disinfection efficiency [5]. This limitation is especially critical for LED with a narrow viewing angle.

Once the trajectories and the incident radiation field are obtained, the UV-dose received by each microorganism can be calculated (Fig. 5 A1-A4). Histogram plots at the reactor outlet are shown together with the dose pathlines.

As expected, the dose increases along the reactor length and with the number of LEDs. The histogram plots include the minimum, percentile 90 and 99, quartiles and averaged accumulated UV dose received by the microorganisms following the different statistical trajectories. All histograms show two regions: A first section of low dose that includes most of the trajectories and characterises the main behaviour of the reactor, and a tail with higher dose values representing the trajectories that are closest to the wall, with the lowest residence time that also receive higher radiation values (due to its closest position to the LEDs).

Most of the particles (75%, quartile 3) have received less than 367, 732, 1306 and 2100 J m^{-2}, for 12, 24, 48, 72 LEDs, respectively. The values of the third quartile correspond approximately to the mean values (376, 747, 1324 and 2131 J $m^{-2,}$ respectively) so that 75% of the particles are below the mean value. The trajectories that exceed these values are those close to the wall. Most relevant is that 25% of the traced trajectories (quartile 1), have received less than 209, 413, 731 and 1182 J m^{-2}, corresponding to approximately 55% of the mean dose value. As observed in Table 3, the relative standard deviation for the received dose decreases as the number of LEDs increases since the incident radiation is more homogeneous, being similar for 48 (A3) and 72 (A4) LEDs.

The logarithmic decay of the concentration of viable microorganisms was used to represent the degree of disinfection for each studied configuration (Fig. 6) by integrating the disinfection kinetics of MS2 virus over each trajectory. Together with the graphical representation, other useful information of the presented methodology is the possibility

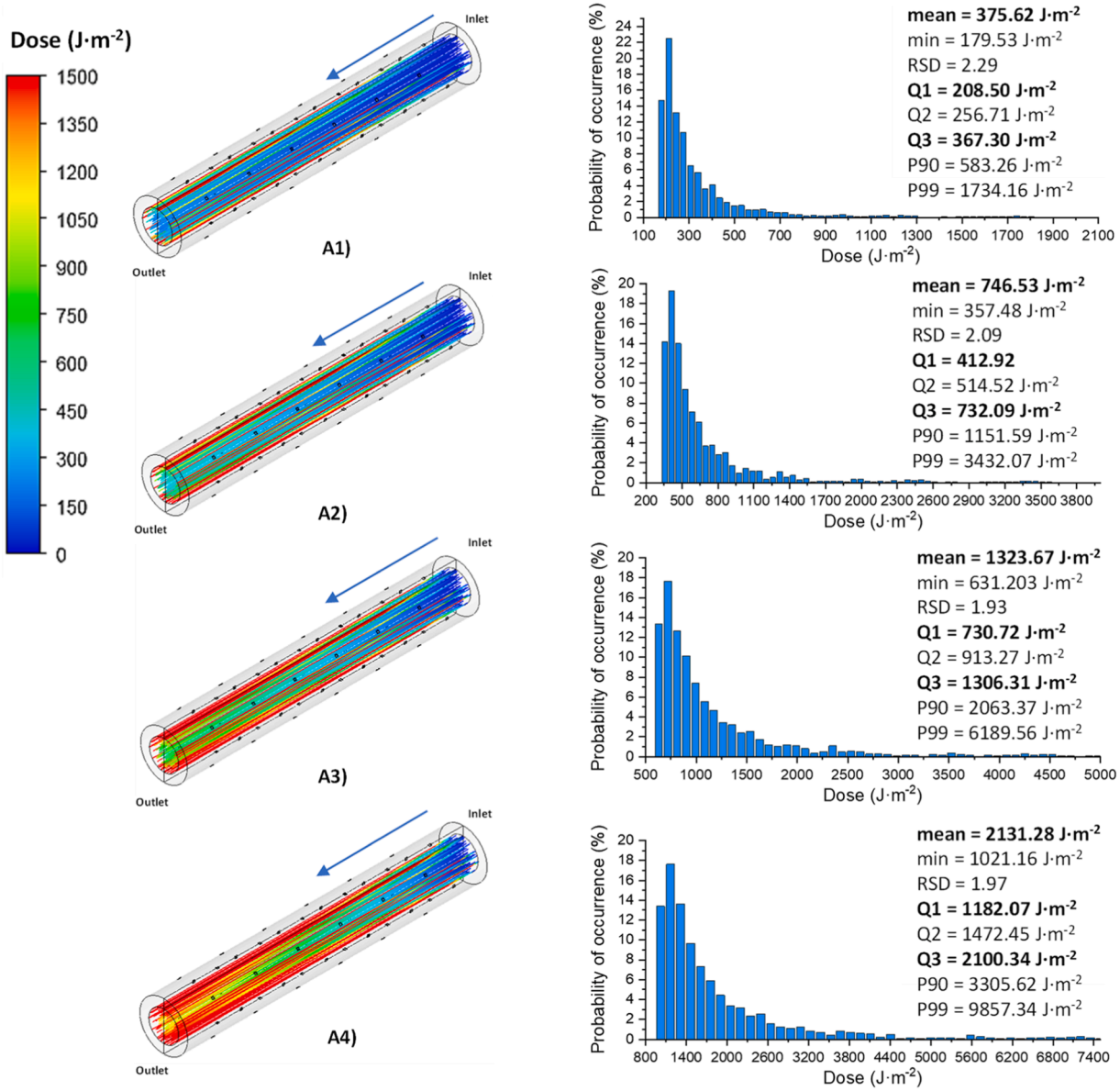

Fig. 5. Left) UV dosage in the tubular reactor illuminated with the four different LED configurations with A1) 12, A2) 24, A3) 48 and A4) 72 LEDs. Note that the upper value of the pathline scale was adjusted to 1500 in all cases to compare the results easier, but higher values of maximum dose are obtained, as shown in the histograms (red colour represents values equal or higher than 1500 J m^{-2}). **Right)** UV dosage histograms at the outlet surface.

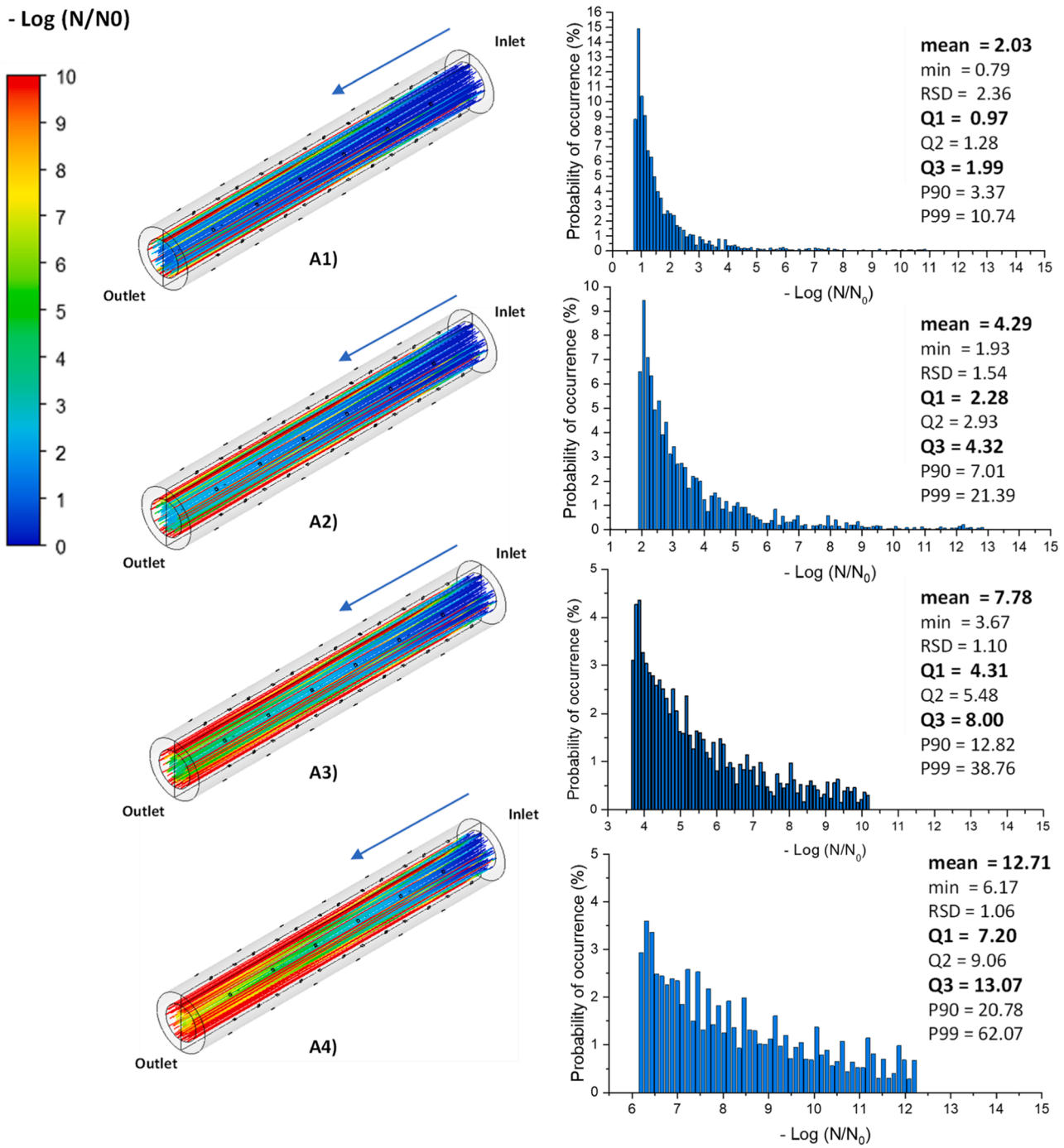

Fig. 6. Left) Microbial inactivation over each trajectory. (A) Tubular reactor illuminated with the four different LED configurations with A1) 12, A2) 24, A3) 48 and A4) 72 LEDs. **Right)** Microbial inactivation histograms at the outlet and summary statistical data.

of obtaining directly the histograms of disinfection, including the minimum values of disinfection reached (most previous reports in the literature only calculated the averaged values).

From Fig. 6 it is easy to choose the number of LEDs or required reactor length to achieve a target level of inactivation. For example, if an average level of 6 log decay of viable microorganism is required, *design A3* (Fig. 6 A3) could be considered an appropriate model, with mean values around 8 log decay in all trajectories reaching the reactor outlet. However, if a level of 6 log decay is the target for all the possible trajectories of microorganisms, *design 4* could be a better option than *design 3*, as *design 3* is not able to guarantee this level for all the microorganisms (quartile 1 value of 4.31 log, while the average value is 8 and a min value of 3.67 log obtained). In the *A3 design* with 48 LEDs, it is observed that 75% of the paths will have a logarithmic inactivation greater than 4.31, which would ensure proper disinfection. Obviously, the *A4 design* will achieve better disinfection in exchange for a higher cost since it has more LEDs.

3.2. Annular reactor

The annular reactor has a more complex flow field, as shown in Fig. 7. Therefore, the effect of the flow rate was studied, with values of the inlet velocity varying according to Table 2. The general trend in the fluid dynamic behaviour is that whereas most of the microorganisms

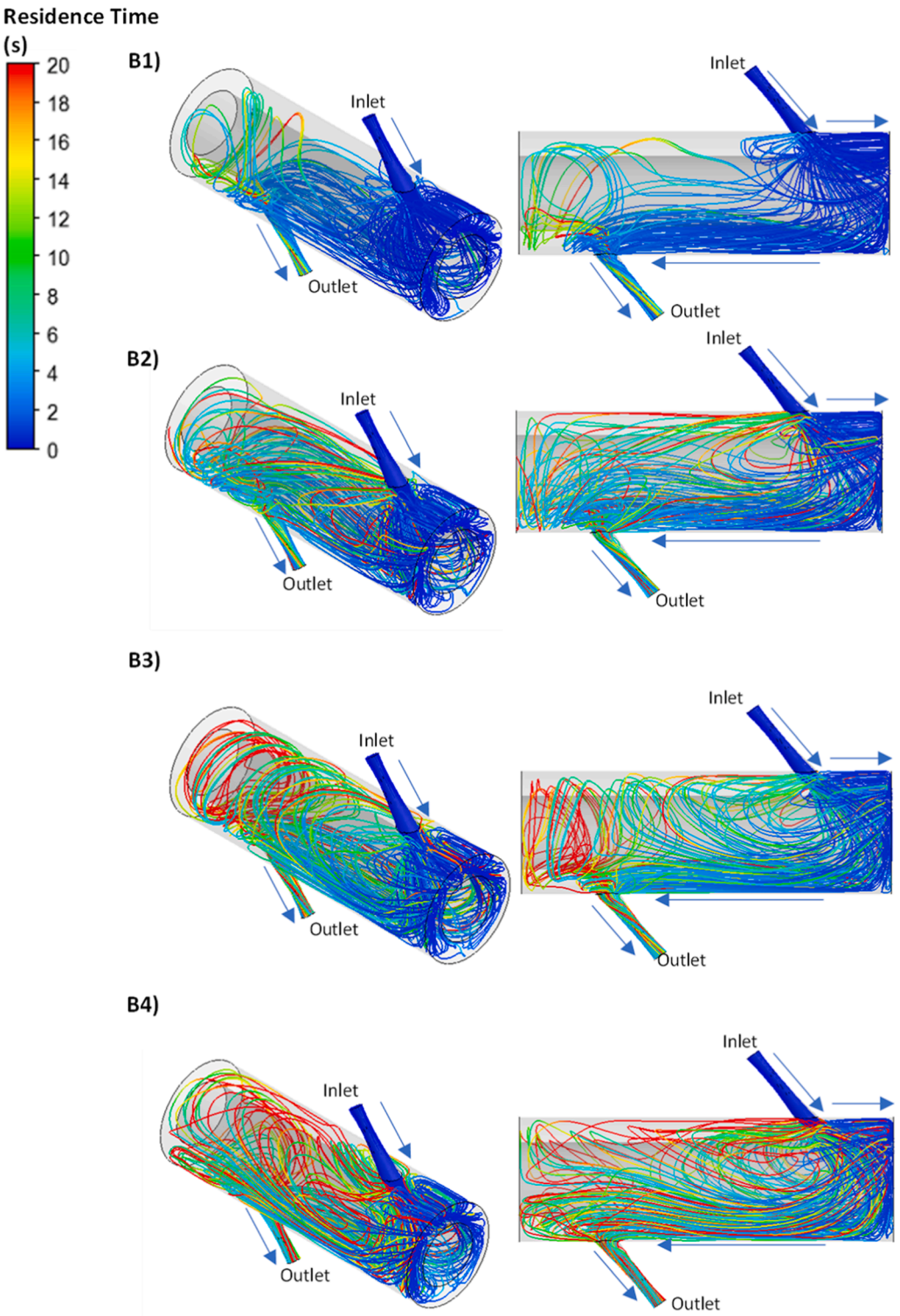

Fig. 7. Residence time distribution for the microbial trajectories in the annular reactor B_V1) 2.62 L·min^{-1}, B_V2) 1.31 L·min^{-1}, B_V3) 0.87 L·min^{-1} and B_V4) 0.66 L·min^{-1}.

reach the outlet of the reactor quickly, some microbial particles are trapped in a dead zone with low velocity (left region in Fig. 7).

For the highest flow rate (Fig. 7 B_V1), the fluid hits the right wall of the reactor, carrying the particles to the reactor outlet at low residence times. When the flow rate is decreased (from 2.62 L·min^{-1} to 0.66 L min^{-1} in Fig. 7 B_V4), the fluid has lesser energy to move pathlines directly to the reactor outlet, the number of pathlines trapped in the dead zone increases, and also appears a transition region between the preferent way to the exit at high velocity and the dead zone with paths surrounding the annular section, showing a quite different fluid-dynamic behaviour. For this low inlet velocity case, the mean residence time is 18.93 s and RSD 1.19 versus 4.22 s and RSD 0.65 for the highest flow rate (see Fig. 8). Note that decreasing the velocity improves the homogeneity in the reactor, getting a narrower relative standard deviation.

As shown in Fig. 8, 75% of the particles leave the reactor in 4.26,

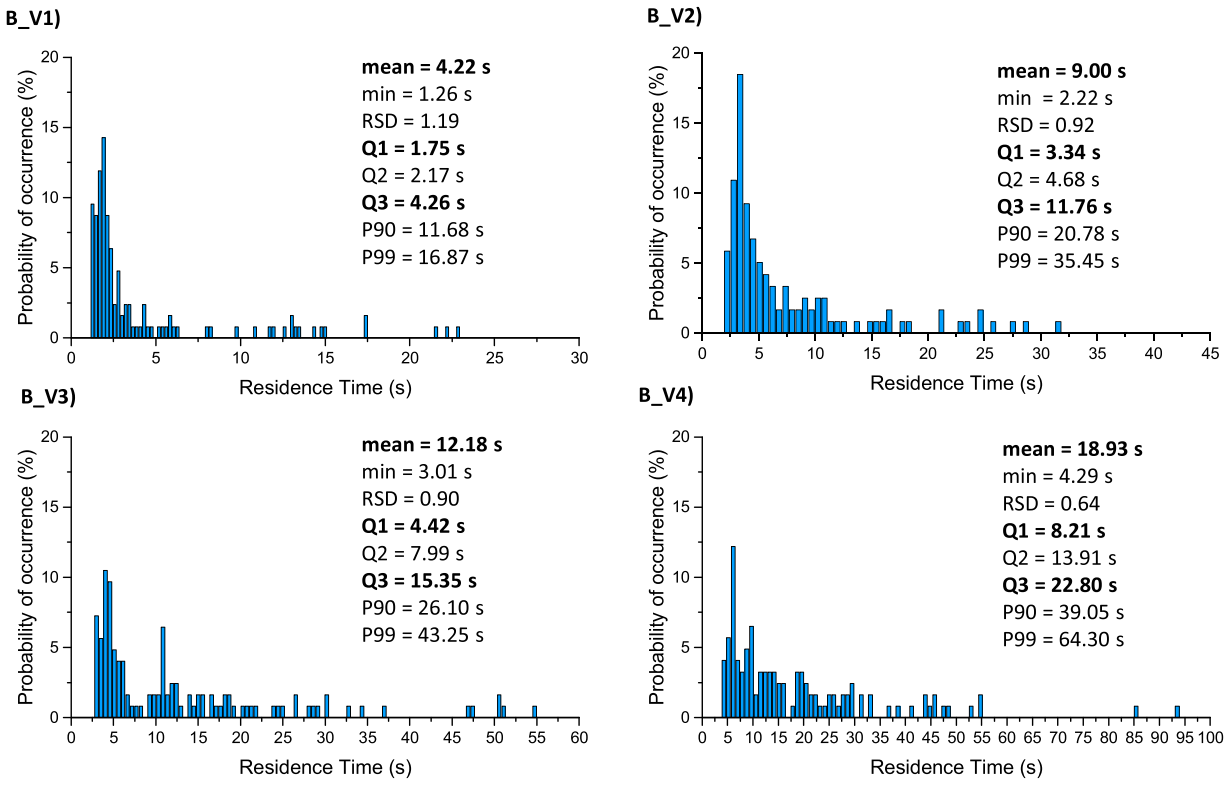

Fig. 8. Residence time distribution in the annular reactor B_V1) 2.62 L·min^{-1}, B_V2) 1.31 L·min^{-1}, B_V3) 0.87 L·min^{-1} and B_V4) 0.66 L·min^{-1}.

11.76, 15.35 and 22.8 s (from 2.62, 1.31, 0.97 and 0.66 L min^{-1}, respectively), remaining in the reactor longer than the average value. This means that around 25% of the particles will receive more radiation than average. However, in this geometry, 50% of the particles have residence times below the average (run through the reactor between half and two-thirds of the average time), and 25% of the particles leave the reactor with residence times between 33% and 42% of the average time.

Fig. 9 shows the radiation distribution and the decrease in radiation with the distance to the tubular mercury fluorescent lamp that illuminates the reactor. The average radiation reaching the reactor wall, its standard deviation, the uniformity index, and the average incident radiation in all the reactor volume are also shown in Fig. 9. The uniformity index in the external reactor wall is 0.95 due to the inhomogeneities caused by the end effects of the tubular lamp. This is a very high value, only reached with LED sources in the tubular reactor when 72 LED were used. This radiation field is kept constant in the fluence calculations carried out in the four scenarios with varying flow rate (Fig. 10).

For all the studied flow rates, the calculated dose is mainly influenced by the great variability in the residence time for each trajectory. The existence of a dead zone and a preferential route to the reactor outlet entail a wide fluence distribution, prevailing over the effect of the relatively low radiation gradients. As expected, the mean dose value increases when decreasing the flow rate with a narrow deviation. Relative standard deviations are practically the same than those obtained in residence time due to the low radial optical path of the reactor.

As shown in Fig. 11, the path the microorganism follows significantly affects the degree of disinfection. Most viral particles leave the reactor without reaching 1 log decay (Fig. 11), with very poor use of the received radiation. In contrast, a small fraction will be trapped in the death zone, decreasing the concentration of viable microorganisms above 4 logs. This complex geometry perfectly exemplifies that the analysis is not straightforward and cannot be exclusively done based on the average values, as typically reported in the literature [22–24]. A quantitative analysis of the cumulative dose in the different trajectories is critical for predicting the disinfection level reached for each microorganism in the reactor.

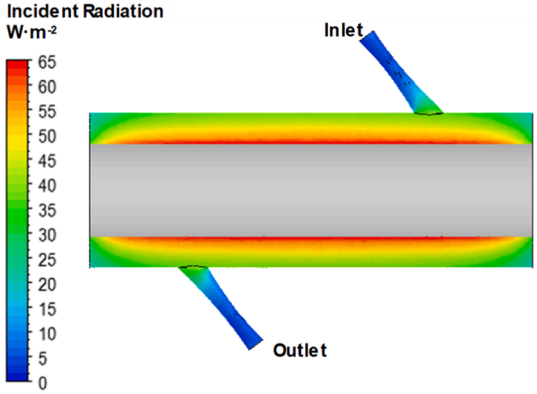

Incident Radiation at the wall (W · m^{-2})	34.98 ± 13.32 %
Volume Average Incident Radiation (W · m^{-2})	44.83
Uniformity Index	0.95

Fig. 9. Incident radiation in the annular reactor (design B).

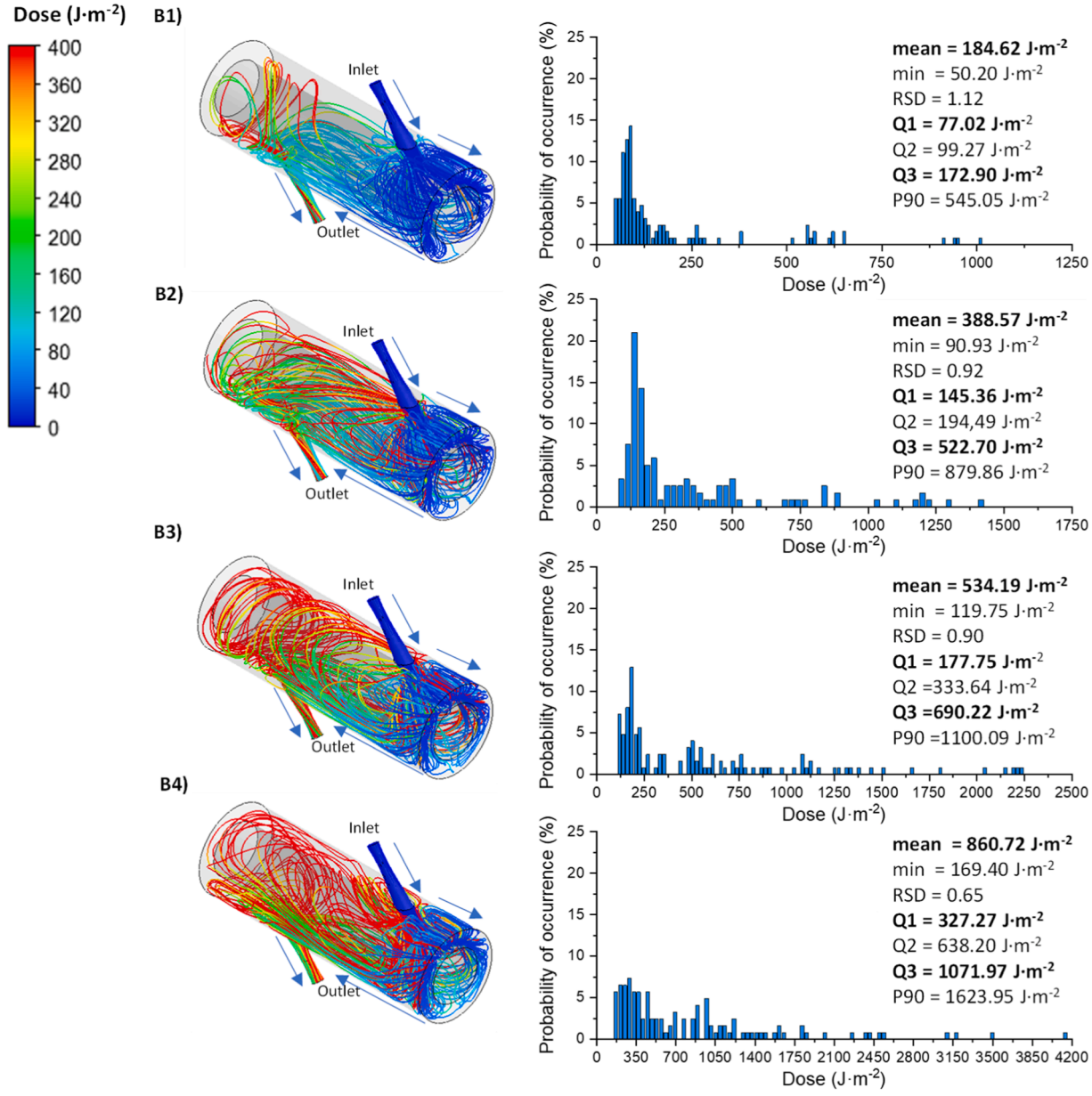

Fig. 10. UV dosage and histograms in the annular reactor with four different flow configurations B_V1) 2.62 L·min^{-1}, B_V2) 1.31 L·min^{-1}, B_V3) 0.87 L·min^{-1} and B_V4) 0.66 L·min^{-1}.

As mentioned above, when the flow decreases, the residence time increases, and so does the degree of disinfection. It can be noted that the disinfection values achieved in this reactor are much lower than in the tubular reactor. In this case, inactivation of 6 log would not be reached in any of the studied conditions. In the best-case scenario, the B_V4 model (mean logarithmic disinfection value of 5.15, RSD 0.17) is the closest to the disinfection values of the A2 design with 24 LEDs (mean logarithmic disinfection value of 4.29, RSD 1.54). Even for longer residence time, 25% of the microorganisms would not have reached 2 log decay..

3.3. Comparison of the studied photoreactors

Comparing these reactors directly is challenging due to the numerous variables affecting them and the fact that they do not operate under the same conditions. However, some general conclusions can still be drawn. Table 5 summarises the results for both systems.

Regarding fluid dynamics, the annular geometry shows a smaller relative deviation of residence time compared with the tubular system (the tubular geometry, with RSD 1.84 can be compared with the case V4 with a similar mean residence time but 0.64 RSD). This is very difficult to estimate without performing these rigorous fluid dynamics calculations due to the more complex flow path caused by the geometry. A higher RSD in residence time obviously lead to a high RSD in the inactivation. Therefore, the velocity profile in the tubular pipe derived from the laminar flow cause a wider distribution of disinfection values achieved, even if the results are flow-averaged.

Regarding the average radiation in the reactor, in the design with 24 LEDs, the reactor receives 40.4 W m^{-2}, which is comparable to the 44.5 W m^{-2} received by the annular reactor. However, the small differences in the dose received (A2: 746.5 ± 2.09 J m^{-2}, tubular with 24 LEDs and V4: 860.7 ± 0.65 J m^{-2} with the tubular lamp), generate notable effects in the degree of disinfection achieved, being the mean value of the log decay 1-log lower in the tubular reactor (4.29 ± 1.54 compared to the 5.15 ± 0.7 achieved in the annular configuration). The annular configuration also has the advantage of a narrower dose

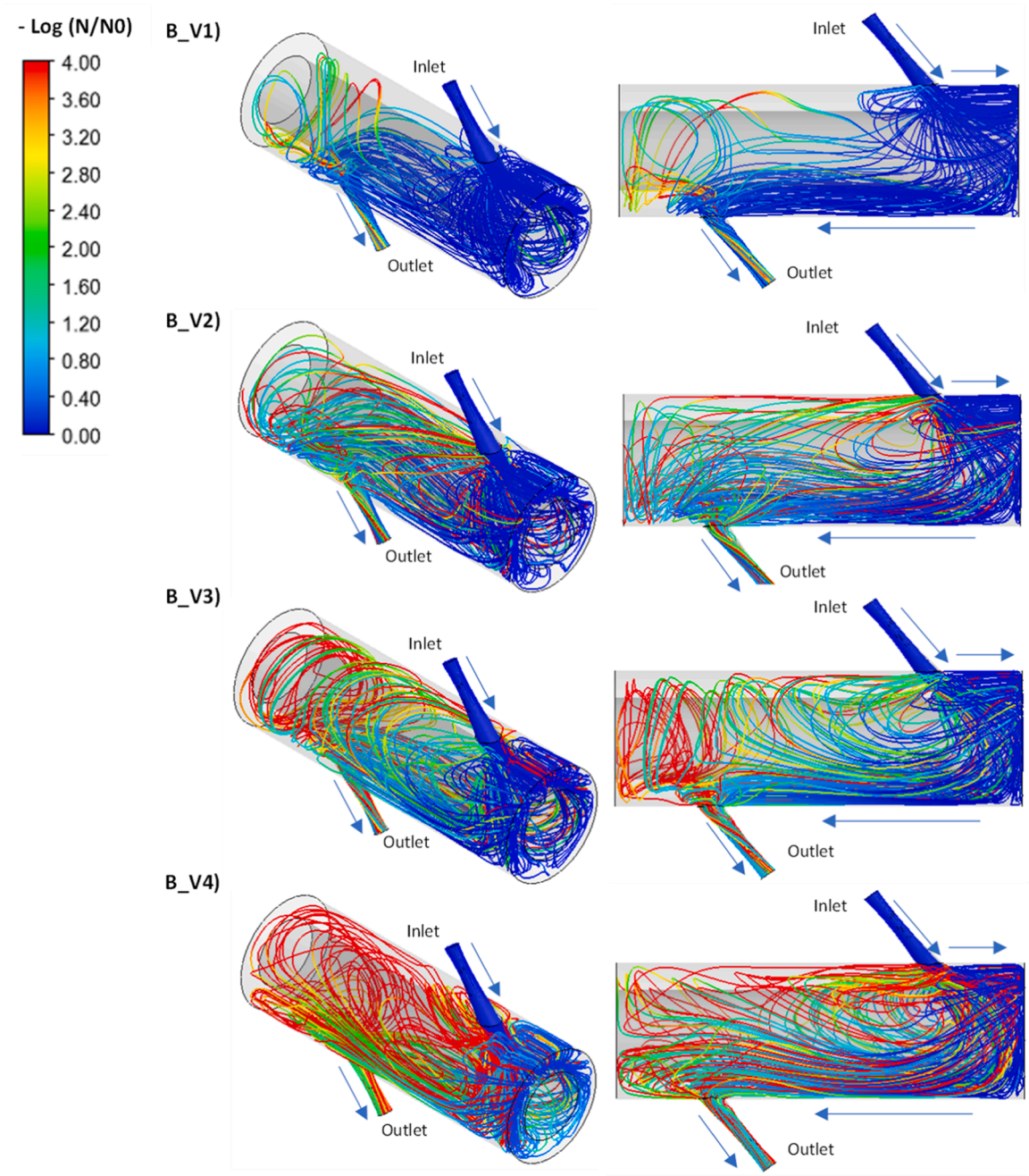

Fig. 11. Microbial inactivation over each trajectory in the annular reactor with four different flow configurations B_V1) 2.62 L·min^{-1}, B_V2) 1.31 L·min^{-1}, B_V3) 0.87 L·min^{-1} and B_V4) 0.66 L·min^{-1}.

distribution which also translates into narrower deviations in the disinfection achieved (53% of microbes are in the Q1 for case A2 vs. 33% in case V4).

The cases A1 (tubular) and V2 (annular) can also be compared since they present similar values of dose. For this comparison, it should be noted that although the residence times and radiation are different in both reactors, similar average dose resulted, as expected, in a very similar degree of disinfection in both reactors, again with a lower variability in the disinfection achieved for the annular geometry.

From this analysis, it can be concluded that the annular configuration is clearly better, especially considering that it can be further optimised. But the most important result of the present study is how the presented novel methodology allows the analysis and optimisation of the reactor design from a rigorous quantitative approach based of the in-situ local inactivation results.

4. Conclusions

This work presented for the first time the direct implementation of microbial inactivation kinetics calculated over the trajectories determined by computational fluid dynamics. This methodology provides the calculation of the internal evaluation of the disinfection process, allowing the graphical identification of problematic regions in photoreactors either derived from inhomogeneous residence time distributions or radiation fields for instance in photocatalytic process. In contrast with the calculation of the average disinfection performance based on the average dose, the calculation of the inactivation rate along the microbial particle trajectories provides detailed information on the statistical distribution of the different inactivation levels, including the percentage of microorganisms that do not reach the disinfection target for the trajectories with shorter residence times.

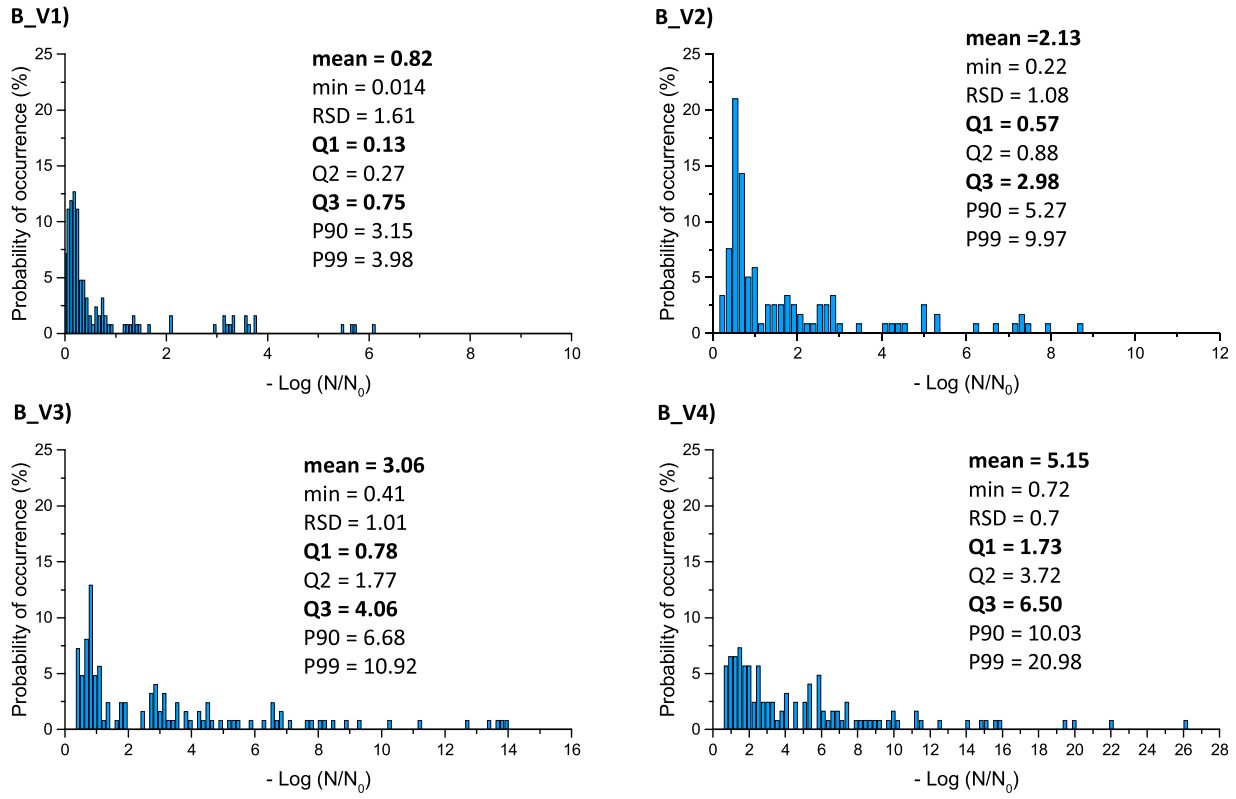

Fig. 12. Microbial inactivation histograms at the outlet and summary statistical data B_V1) 2.62 L·min^{-1}, B_V2) 1.31 L·min^{-1}, B_V3) 0.87 L·min^{-1} and B_V4) 0.66 L·min^{-1}.

Table 5
Comparison of the studied reactors.

Tubular reactor				Annular reactor			
	Residence Time ± RSD (s)	Dose ± RSD (J m^{-2})	-Log (N/N0) ± RSD		Residence Time ± RSD (s)	Dose ± RSD (J m^{-2})	-Log (N/N0) ± RSD
A1	18.31 ± 1.84	375.6 ± 2.29	2.03 ± 2.36	V1	4.22 ± 1.19	184.62 ± 1.12	0.82 ± 1.61
	Q1 = 10.43	Q1 = 208.5	Q1 = 0.97		Q1 = 1.75	Q1 = 77.02	Q1 = 0.13
A2	18.31 ± 1.84	746.5 ± 2.09	4.29 ± 1.54	V2	9.00 ± 0.92	388.6 ± 0.92	2.13 ± 1.08
	Q1 = 10.43	Q1 = 412.9	Q1 = 2.28		Q1 = 3.34	Q1 = 145.4	Q1 = 0.57
A3	18.31 ± 1.84	1323.7 ± 1.93	7.78 ± 1.10	V3	12.18 ± 0.90	534.2 ± 0.9	3.06 ± 1.01
	Q1 = 10.43	Q1 = 730.72	Q1 = 4.31		Q1 = 4.42	Q1 = 177.75	Q1 = 0.78
A4	18.31 ± 1.84	2131.3 ± 1.97	12.71 ± 1.06	V4	18.93 ± 0.64	860.7 ± 0.65	5.15 ± 0.7
	Q1 = 10.43	Q1 = 1182.07	Q1 = 7.20		Q1 = 8.21	Q1 = 327.27	Q1 = 1.73

A first case of a tubular reactor with a simple geometry but complex radiation field derived from the use of LED sources showed the importance of studying the homogeneity of the light delivered to the system. In the studied system, a minimum of 48 LEDs were needed to obtain a homogeneity similar to a tubular mercury lamp. When coupled with the velocity gradients, the co-existence of higher incident radiation together with much lower velocity values in zones close to the reactor wall leads to extremely high inactivation values in comparison with the bulk of the reactor volume, even when flow-weighted values are analysed.

The second case of an annular reactor illuminated with a tubular lamp presented a simpler light distribution but a much more complex flow pattern affected by the flow rate value. A preferential path and a clearly differentiated dead zone were observed for the highest studied velocity, leading to very different inactivation values depending on the microorganism's trajectory. Inactivation homogeneity can be improved by reducing the flow rate, also increasing the residence time and average disinfection performance.

We consider that the tool presented in this work is a useful and easy to implement step for improving the design of reactors in UV disinfection, since it allows the graphic visualisation of the disinfection performance inside the reactor together with the distribution of radiation and residence time.

The developed methodology demonstrates its usefulness for the optimisation of the performance of photoreactors for water disinfection. Independently on the complexity of the reactor geometry, it has been proved the importance of taking into account local velocities in the design of single-pass photoreactors to ensure that a sufficient dose is delivered.

Although this work has been focused on the inactivation of viral particles as a showcase scenario, its application to other microbial pathogens (bacteria, protozoa, etc) only requires a change in the kinetic parameters of the inactivation.

CRediT authorship contribution statement

Cintia Casado: Conceptualization, Software, Validation, Writing – original draft. Writing – review & editing. **Verónica Yunta:** Investigation, Software, Formal analysis, Writing – original draft. **Javier**

Marugán: Conceptualization, Supervision, Funding acquisition, Validation, Writing – review & editing.

Declaration of Competing Interest

The authors declare that they have no known competing financial interests or personal relationships that could have appeared to influence the work reported in this paper.

Data Availability

The author have shared the code in the manuscript, if necessary other data available on request.

Acknowledgements

The authors gratefully acknowledge the financial support of the Spanish State Research Agency (AEI) and the Spanish Ministry of Science and Innovation through the project AQUAENAGRI (PID2021–126400OB-C32), the European Union's Horizon 2020 research and innovation programme in the frame of the HYSOLCHEM project (GA 101017928) and the Community of Madrid in the frame of the Multiannual Agreement with the Rey Juan Carlos University "Encouragement for research by young doctors" (M2738 SAFECAT-Agua).

APPENDIX A

User-defined function to compute the inactivation over each trajectory.

```
#include "udf.h".
#include"sg_disco.h".
DEFINE_INIT(fluence_setup2,domain).
/*Used to specify a set of initial values for the solution, it is called immediately after the solver performs the default initialisation.
{/*It is necessary to add 4 memory units* /.
if (NULLP(user_particle_vars)) Init_User_Particle_Vars();.
/*now set the name and label* /.
strcpy(user_particle_vars[0].name,"fluence-dose");.
strcpy(user_particle_vars[0].label,"Fluence Dose");.
strcpy(user_particle_vars[1].name,"fluence-dose-0");.
strcpy(user_particle_vars[1].label,"Fluence Dose 0");.
strcpy(user_particle_vars[2].name,"survival");.
strcpy(user_particle_vars[2].label,"Survival");.
strcpy(user_particle_vars[3].name,"log_inact");.
strcpy(user_particle_vars[3].label,"Log_inact");.
}.
DEFINE_DPM_SCALAR_UPDATE(fluence_dose2,cell,thread,initialize,p).
/* update the user scalar variables * /.
{real IncRad = C_DO_IRRAD(cell,thread,0);.
if (initialise).
{P_USER_REAL(p,0) = 0.0;.
P_USER_REAL(p,1) = IncRad;.
P_USER_REAL(p,2) = 1.0;.
P_USER_REAL(p,3) = 0.0;}.
else.
{P_USER_REAL(p,0) += P_DT(p) * (P_USER_REAL(p,1) + IncRad) / 2;.
/* save current variable for start of next step * /.
P_USER_REAL(p,1) = IncRad;.
P_USER_REAL(p,2) = MIN(1.0,pow(10.0,(−0.0064 * (P_USER_REAL(p,0))+0.361)));.
P_USER_REAL(p,3) = -log10(P_USER_REAL(p,2));}.
}.
DEFINE_DPM_OUTPUT(fluence_output2,header,fp,p,thread,plane).
/* write the value of the variables in the particles on a surface* /.
{char name[100];.
if (header).
{if (NNULLP(thread)).
par_fprintf_head(fp,"(%s %d)\n",THREAD_HEAD(thread)->.
dpm_summary.sort_file_name,13);.
else.
par_fprintf_head(fp,"(%s %d)\n",plane->sort_file_name,13);.
par_fprintf_head(fp,"(%10 s %10 s %10 s %10 s %10 s %10 s %10 s".
" %10 s %10 s %10 s %10 s %10 s %10 s %s)\n",
"X","Y","Z","U","V","W","diameter","T","mass-flow",
"time","fluence","survival","log-inact","name");}.
else.
{sprintf(name,"%s:%d",P_INJECTION(p)->name,p->part_id);.
par_fprintf(fp,
"%d %d ((%10.6 g %10.6 g %10.6 g %10.6 g %10.6 g %10.6 g ".
"%10.6 g %10.6 g %10.6 g %10.6 g %10.6 g %10.6 g %10.6 g) %s)\n",
P_INJ_ID(P_INJECTION(p)), p->part_id,
P_POS(p)[0], P_POS(p)[1], P_POS(p)[2],
P_VEL(p)[0], P_VEL(p)[1], P_VEL(p)[2],
P_DIAM(p), P_T(p), P_FLOW_RATE(p), P_TIME(p),
P_USER_REAL(p,0), P_USER_REAL(p,2), P_USER_REAL(p,3), name);}.
```

References

[1] M.W. LeChevallier, Water treatment and pathogen control: process efficiency in achieving safe drinking-water, IWA Publ. 12 (2004), https://doi.org/10.2166/9781780405858.

[2] A. Zyara, E. Torvinen, A.-M. Veijalainen, H. Heinonen-Tanski, The effect of UV and combined chlorine/UV treatment on coliphages in drinking water disinfection, Water 8 (2016) 130, https://doi.org/10.3390/w8040130.

[3] H. Cao, B. Deng, J. Hong, J. Xue, F. Chang, Numerical simulation of the arrangement of baffles on radiation distribution and disinfection in UV reactors, Chem. Eng. Technol. 39 (2016) 108–114, https://doi.org/10.1002/ceat.201500151.

[4] B.A. Wols, J.A.M.H. Hofman, W.S.J. Uijttewaal, L.C. Rietveld, J.C. van Dijk, Evaluation of different disinfection calculation methods using CFD, Environ. Model. Softw. 25 (2010) 573–582, https://doi.org/10.1016/j.envsoft.2009.09.007.

[5] M. Somer, C. Pablos, R. van Grieken, J. Marugán, Influence of light distribution on the performance of photocatalytic reactors: led vs mercury lamps, Appl. Catal. B Environ. 215 (2017), https://doi.org/10.1016/j.apcatb.2017.05.048.

[6] J.J. Ducoste, D. Liu, K. Linden, Alternative approaches to modeling fluence distribution and microbial inactivation in ultraviolet reactors: Lagrangian versus Eulerian, J. Environ. Eng. 131 (2005) 1393–1403, https://doi.org/10.1061/(ASCE)0733-9372(2005)131:10(1393).

[7] R. B.E, S. Chengyue, N. Zorana, L. Lian-Shin, A. L.D, R.J. Paul, R. Katherine, G. Gérald, E. B.D, F. Shiyue, G. Yousheng, J. Kristofer, G. Nilupa, Dyed microspheres for quantification of UV dose distributions: photochemical reactor scharacterisation by lagrangian actinometry, J. Environ. Eng. 132 (2006) 1390–1403, https://doi.org/10.1061/(ASCE)0733-9372(2006)132:11(1390).

[8] A. Munoz, S. Craik, S. Kresta, Computational fluid dynamics for predicting performance of ultraviolet disinfection – sensitivity to particle tracking inputs, J. Environ. Eng. Sci. 6 (2007) 285–301, https://doi.org/10.1139/s06-045.

[9] D. Lyn, I. Blatchley, Numerical computational fluid dynamics-based models of ultraviolet disinfection channels, J. Environ. Eng. 131 (2005) 838–849, https://doi.org/10.1061/(ASCE)0733-9372(2005)131:6(838).

[10] D.A. Sozzi, F. Taghipour, Computational and experimental study of annular photoreactor hydrodynamics, Int. J. Heat. Fluid Flow. 27 (2006) 1043–1053, https://doi.org/10.1016/j.ijheatfluidflow.2006.01.006.

[11] H. Sobhani, H. Shokouhmand, Effects of number of low-pressure ultraviolet lamps on disinfection performance of a water reactor, J. Water Process Eng. (2017), https://doi.org/10.1016/j.jwpe.2017.08.021.
[12] C. Casado, J. Marugán, R. Timmers, M. Muñoz, R. van Grieken, Comprehensive multiphysics modeling of photocatalytic processes by computational fluid dynamics based on intrinsic kinetic parameters determined in a differential photoreactor, Chem. Eng. J. 310 (2017) 368–380, https://doi.org/10.1016/j.cej.2016.07.081.
[13] ANSYS®, ANSYS User and Theory Guide, Release 14.5, in: ANSYS Fluent, (2012).
[14] R.K. Saha, M. Ray, C. Zhang, Computational fluid dynamics simulation and parametric study of an open channel ultra-violet wastewater disinfection reactor, Water Qual. Res. J. 50 (2014) 58–71, https://doi.org/10.2166/wqrjc.2014.034.
[15] J. Chen, B. Deng, C.N. Kim, Computational fluid dynamics (CFD) modeling of UV disinfection in a closed-conduit reactor, Chem. Eng. Sci. 66 (2011) 4983–4990, https://doi.org/10.1016/j.ces.2011.06.043.
[16] C. Casado, Á. García-Gil, R. van Grieken, J. Marugán, Critical role of the light spectrum on the simulation of solar photocatalytic reactors, Appl. Catal. B Environ. 252 (2019) 1–9, https://doi.org/10.1016/J.APCATB.2019.04.004.
[17] M. Pirnie, K.G. Linden, J.P. Malley, D. Schmelling, O. of W. USA, Ultraviolet disinfection guidance manual for the final long term 2 enhanced surface water treatment rule: EPA 815-R-06–007, EPA. (2006).
[18] D. Liu, C. Wu, K. Linden, J. Ducoste, Numerical simulation of UV disinfection reactors: evaluation of alternative turbulence models, Appl. Math. Model. 31 (2007) 1753–1769, https://doi.org/10.1016/J.APM.2006.06.004.
[19] J. Marugán, R. van Grieken, C. Sordo, C. Cruz, Kinetics of the photocatalytic disinfection of Escherichia coli suspensions, Appl. Catal. B Environ. 82 (2008) 27–36, https://doi.org/10.1016/j.apcatb.2008.01.002.
[20] M. Peleg, Microbial dose-response curves and disinfection efficacy models revisited, Food Eng. Rev. 13 (2021) 305–321, https://doi.org/10.1007/S12393-020-09249-6.
[21] H.S. Fogler, Essentials of Chemical Reaction Engineering: Essenti Chemica Reactio Engi, Pearson Education, 2010.
[22] H. Sobhani, H. Shokouhmand, Effects of number of low-pressure ultraviolet lamps on disinfection performance of a water reactor, J. Water Process Eng. 20 (2017) 97–105, https://doi.org/10.1016/j.jwpe.2017.08.021.
[23] T. Sultan, Z. Ahmad, K. Hayat, I.A. Chaudhry, Computational analysis of three lamp close conduit water disinfection UV reactor, Int. J. Environ. Sci. Technol. 19 (2022) 4393–4406, https://doi.org/10.1007/s13762-021-03344-9.
[24] R.K. Saha, M. Ray, C. Zhang, R. Kumar, S.C. Zhang, Computational fluid dynamics simulation and parametric study of an open channel ultra-violet wastewater disinfection reactor, Iwaponline.Com 50 (2015) 58–71, https://doi.org/10.2166/wqrjc.2014.034.